Spat. Inf. Res. (2017) 25:293–302
DOI 10.1007/s41324-017-0100-z

Impact of rapid urbanisation on land cover in Istanbul Province

Fatih Kara[1] · **Arif Keçeli**[2]

Received: 12 December 2016 / Revised: 4 April 2017 / Accepted: 6 April 2017 / Published online: 13 April 2017

Abstract Since the industrial revolution, rapid urban sprawl has been one of the main characteristics of urbanised areas worldwide. The main objective of this study was to detect, quantify and characterise the changes in land use/land cover (LULC) in Istanbul Province between 2003 and 2015 using a hybrid geographic information systems (GIS)-remote sensing method. Landsat Thematic Mapper and operational land imager images were co-registered and classified using object-based image classification techniques and visual analysis. Land cover maps were rasterized at the same spatial resolution (30 m) in a GIS environment and the same legend was used for both land cover maps. Urbanised areas and other LULC types were determined for the years 2003 and 2015. The extent and spatial distribution of a number of LULC classes in Istanbul changed between 2003 and 2015. Settlement areas increased by 20,464.1 ha in only 12 years and 2529.89 ha of forested land was destroyed for construction of a new highway. Moreover, forests and agricultural areas became highly fragmented. This study confirms the accuracy of the hybrid GIS-remote sensing method. Moreover, the resulting data highlights the extent of the recent rapid land degradation in Istanbul and calls attention to the importance of protecting the natural ecosystems in this area.

✉ Fatih Kara
fatihkara@fatih.edu.tr

Arif Keçeli
keceli@mehmetakif.edu.tr

[1] Department of Geography, Faculty of Arts and Science, Fatih University, Buyukcekmece, 34500 Istanbul, Turkey

[2] Department of Geography, Faculty of Arts and Science, Mehmet Akif University, Istiklal Yerleskesi, 15030 Burdur, Turkey

Keywords Rapid urbanisation · Remote sensing · Land use/land cover change · Istanbul

1 Introduction

Population flow from rural to urban areas increased dramatically as a result of the industrial revolution in the early nineteenth century. Such population movements have negatively affected natural ecosystems in a variety of ways, for example, by increasing pollution, forest degradation, landscape fragmentation and surface runoff [1–3]. It is suggested that land use/land cover (LULC) change is one of the major components of global change and may have a greater effect than climate change [4]. Indeed, changes to land surfaces influence climate and impact ecosystems and goods [5]. Very different forms of LULC changes have occurred over time [6], though the decline in forest and green space areas is the most important negative type of change-impacted land degradation [7].

Temporal changes in LULC are critical aspects of sustainable planning and development [8] due to the immediate impacts of LULC on the major components of natural ecosystems [9, 10]. Remote sensing (RS) images are a valuable resource for assessing the magnitude and patterns of change through LULC change analysis [11]. Landsat 4/5 TM and Landsat 8 OLI images are commonly used for monitoring LULC changes due to their relatively high spatial resolution and availability [12, 13]. LULC changes in the same location can be detected by classifying before and after images of the same area [14, 15]. For example, Dewan and Yamaguchi [16] examined LULC patterns in the Dhaka Metropolitan area over 45 years in the context of sustainable land use and environmental planning, and Wan et al. [17] investigated comparative dynamic LULC

changes using GIS procedures and remotely-sensed satellite images in the Jiansanjiang region of China for natural resource conservation.

Various change detection methods have been developed for different purposes, such as assessment of rapid urbanisation [18, 19], vegetation cover changes [20, 21], deforestation [22, 23], and monitoring the environment [24, 25]. Several algorithms have been proposed for change detection studies and can be placed into two major categories: (1) pixel-to-pixel comparison of satellite imagery and (2) post-classification comparison [26]. Support vector machine [27], image algebra [28], image classification [29], change vector analysis [30], image transformation [31] and feature extraction [32] are the most widely used techniques for detection of temporal LULC changes.

In addition to these methods, post-classification comparison is another common method that enables comparison of classified "before" and "after" images which are imagery of same geographic location belong to different dates [33, 34]. Taha [35] investigated urbanisation encroachment in the Nile River delta using fuzzy post classification comparison. Colditz et al. [36] studied the potential effects of multi-resolution post-classification changes in the Alvarado mangrove area of the Mexican Gulf Coast. Teng et al. [37] applied post-classification comparison and image differencing methods to multitemporal satellite images of central Taiwan.

The population of Istanbul has increased very rapidly due to migrations in last 15 years. According to the address-based census system [38], the population of Istanbul was 10,072,447 in 2000 and increased to 14,657,434 in 2015. Therefore, LULC changes in Istanbul Province need to be assessed using spatial techniques. In this study, Landsat satellite imagery, remote sensing and GIS methods were combined with object-based classification and post-classification comparison techniques to measure the rates of urbanisation and urban sprawl and assess the impact of urbanisation on the environment and vegetation cover by measuring LULC changes in Istanbul Province between 2003 and 2015.

2 Data and methods

Rapid urbanisation and LULC changes were detected by classification of "before (2003 mosaic)" and "after (2015 mosaic)" Landsat imagery. Each data set was composed from Landsat 5 TM and Landsat 8 OLI satellite images, which have the same spatial resolution (30 m) but a different spectral resolution (Table 1).

In order to generate highly accurate land cover maps of the study area for the years of 2003 and 2015, pre-processing steps including atmospheric corrections and rescaling were applied to all Landsat scenes. In the second step, the images were classified by spectral segmentation and object based image classification methods. High resolution maps and images were used as auxiliary data to determine LULC classes. In the final step, a confusion (error) matrix was produced to evaluate the classification results.

2.1 Study area

The study area, Istanbul Province, lies in North Western Turkey. The city straddles the Çatalca Peninsula to the West (Europe) and Kocaeli Peninsula to the East (Asia), with the two parts of the city divided by the Bosporus. The study area is located between the longitudes of 28°01′–29°55′ east and latitudes of 40°28′–41°33′ north and covers an area of 5.461 km^2 including lake surfaces (Fig. 1).

Istanbul has a transitional climate that is affected by the Black Sea from the North and Mediterranean Sea from the South. The average annual temperature is 14.3 °C and the monthly average temperature ranges from 5.8 °C in January to 23.6 °C in August. Annual total precipitation is 749.5 mm [39] and due to the impact of the Mediterranean Sea, most precipitation occurs in winter and least in summer. The natural vegetation cover of Istanbul is composed of forest, maquis shrubland, adapted pseudo-maquis and shoreline plants [40]. Common tree species include oak, chestnut, beech, hornbeam, maple, Mediterranean cypress and pine (*Pinus pinea*); forests are widespread, especially in the northern parts of the study area.

Istanbul Province lies on two abrasion plateaus, the Kocaeli and Çatalca peninsulas. The area has a moderate rugged terrain with no abrupt or massive changes in the small-scale valleys, plains, hills and highlands. The highest hills are mainly located on the Asian side of Istanbul and have an average altitude of 350 m; elevation generally increases from west to east throughout the province. Aydos Mountain is the highest peak in the study area at 537 m. There are three large lakes in Istanbul Province, Terkos, Büyükçekmece and Küçükçekmece, which formed as lagoons.

The population of the study area was 10,072,447 in 2000 and 14,657,434 in 2015 (TUIK 2016). Istanbul is composed of 39 sub-provinces, 25 of which are located on the European side; almost two-thirds of the population live on this side of the city. Istanbul is the largest urban area and major centre of industry, commerce, culture, education and business in Turkey. The city is the geographic connection point of Europe and Asia and has important roads and highways which play major roles in transit transportation. Population of Istanbul is increasing very rapidly due to migration pressure from the other cities of Turkey and it is important to assess LULC changes in the city by spatial techniques.

Table 1 Characteristics of the satellite images used as primary data in this study

Scene ID	Instrument	Date acquired	Spectral resolution	Spatial resolution
LT51800312003184MTI01	Landsat 5 TM	03.07.2003	8-bit	30 m
LT51800322003184MTI01	Landsat 5 TM	03.07.2003	8-bit	30 m
LC81800312015137LGN00	Landsat 8 OLI	17.05.2015	12-bit	30 m
LC81800322015137LGN00	Landsat 8 OLI	17.05.2015	12-bit	30 m

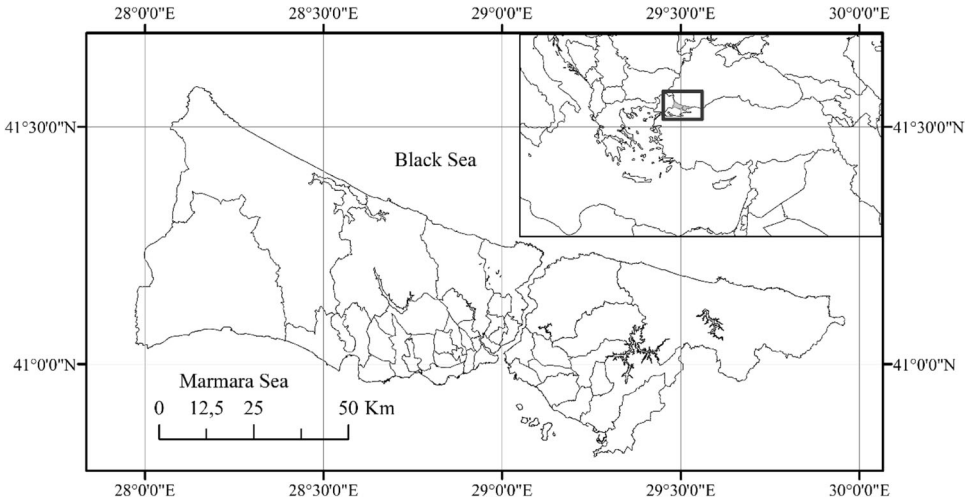

Fig. 1 Location of the study area, Istanbul Province

2.2 Pre-processing

Mosaic images were prepared for the years of 2003 and 2015 and then classified via an object-based image analysis technique (Table 1). The pre-processing steps including all image preparation stages such as geometrical setup and atmospheric correction were applied to mosaicked images before classification.

The first mosaic (for 2003) image was generated from two Landsat 5 TM images taken in 2003. Six of the seven bands in the TM images, except for the thermal band (band 6), were stacked and multispectral images were created. The thermal band of the sensor was not included due to its lower spatial resolution (120 m) in comparison with the other bands (30 m; USGS 2015a).

The two multispectral images were mosaicked and a single multispectral image covering the entire study area was generated with a spatial resolution of 30 m. Mosaic images usually contain artefacts due to variations in the atmospheric conditions on the date of acquisition. Therefore, a colour balancing algorithm was applied to remove atmospheric effects while mosaicking: a histogram matching procedure was applied to achieve image-to-image color correction [41]. This technique is useful for matching satellite images of the same or adjacent scenes taken on different dates under different atmospheric conditions. The histogram matching technique determines a lookup table to approximately convert the histogram of one image to the histogram of another image [42]. Master and slave images were determined and the histograms of these images were computed and compared. Band-to-band histogram matching was performed to remove color differences between the images and create a single image covering the entire study area at the end of the mosaicking procedure. Finally, the mosaic image was subset by the province borders of Istanbul and prepared for atmospheric correction.

The second mosaic (for 2015) image was prepared using exactly the same methods/techniques as the before image. Six bands of Landsat OLI images acquired of Istanbul on two dates in 2015 were stacked and multispectral images were created. Bands 2, 3, 4, 5, 6 and 7 were selected and stacked to create multispectral images corresponding to the same scenes as the Landsat 5 TM images. The other bands of the OLI sensor were excluded to create images with the same spatial and spectral properties [43] as the 2003 mosaic image.

Different atmospheric conditions in illumination, scattering and absorption may produce alterations in radiance values that are normally not associated with the reflectance values of land cover classes [44]. The main principle of determining LULC changes by remote sensing techniques is that the radiance differences associated with LULC changes are larger than the radiance changes due to variations in atmospheric conditions [45]. Seasonal effects can lead to errors in change detection studies and satellite images captured in clear weather conditions in the same season have to be selected to mitigate uncertainties due to

inter-annual variability [46, 47]. All TM and OLI images were subjected to a dark object subtraction (DOS) procedure [23–48] to obtain reflectance images. DOS is a simple, widely used image-based atmospheric correction method [42] that was used to clean-up each band of the TM and OLI images to remove atmospheric haze. The DOS method accepts that the sunshine reflected by dark objects is one of the major components of atmospheric scattering. This method assumes some unwanted atmospheric effects, such as haze, can be eliminated by determining the darkest pixel value of a band (or image) and subtracting this value from each pixel value in each band.

2.3 Image classification

For change detection applications, satellite images should be acquired by the same sensor and at the same time of the year [49]. Different sensors can have different spatial and radiometric resolutions, thus pixel-by-pixel (per pixel) comparisons of satellite images cannot be achieved. In this study, the scenes of the 2003 mosaic image were acquired using a Landsat TM sensor with 30 m spatial resolution and 8-bit radiometric resolution. The scenes of the 2015 mosaic image were acquired using a Landsat OLI sensor with 30 m spatial resolution (without panchromatic band) and 12-bit radiometric resolution. A per pixel classification technique was not applied in this study, though the 2015 mosaic image was rescaled to 8-bit to equalise the segmentation conditions.

Image segmentation was the first step of object-based classification. The image segmentation process was performed using eCognition 8.9 software [50, 51], via an area-merging technique achieved by selection of a random pixel and determination of segments with connection to neighbouring pixels due to scale, colour (DN values), homogeneity criteria and shape. At each step, image objects were merged and converted to a new larger object. The merging decision based on local homogeneity criteria consists of 'fit' or 'fit not' criterion but also merges the cost representing 'degree of fitting' (1). The degree of fitting *h,* for a d-dimensional feature spaces is calculated as:

$$h = \sqrt{\sum_{d} (\int_{1d} - \int_{2d})} \tag{1}$$

The ultimate goal of this 'multi-resolution segmentation' method is to build hierarchical sets of image objects with different spatial resolutions [52]. The multi-resolution segmentation approach produced more than 20,000 segments for both the TM and OLI images and all of these segments were classified according to the National Land Cover Definition (NLCD) system of the United States Geological Survey (USGS) defined in 1992 [53]. Nine of the 21 classes of this classification system were determined from the 30 m spatial resolution Landsat images.

Visual analysis is a strong and highly accurate way of evaluating segments [50]. The segments of the Landsat TM images were classified by visual analysis of high-resolution satellite images such as a IKONOS pan-sharpened 2006 image with 1 m resolution, IKONOS multi-spectral 2008 image with 4 m resolution, aerial photos and municipal maps, along with the 2003 Landsat TM image itself. The segments of the 2015 Landsat OLI image were classified by visual analysis of ArcGIS base maps (2008 IKONOS images with 1 m resolution), Google Earth and the OLI image itself.

2.4 Change detection

It is important to accurately inventory a number of biophysical and human-made features so that physical- and human-related processes can be better understood [54, 55]. Multi-temporal data sets (satellite images) may be acquired for the same geographic location by the repetitive surface coverage of satellites. These data enable the adoption of different types change detection techniques such as change vector analysis (CVA), principal component analysis (PCA), image differencing and multi-date image classification [56, 57].

Post-classification comparison (PCC) of the classified Landsat images was used as the change detection technique in this study. PCC is widely-used in change detection studies [58, 59]. This method is based on the comparison of land cover classes at the pixel scale and is applied by subtraction of one image from another. A change matrix was developed and change areas can be displayed along with LULC classes [49–60]. The main advantage of this method is that it provides a complete change matrix between study dates [61, 62]. As it classifies each image independently, PCC can greatly reduce the error in change detection studies; however, the accuracy of this method depends on the accuracy of classification [58].

If the accuracy of the transitions is of interest as well as assigning classes, the transition error matrix is the most informative tool [63]. In this study, the PCC error matrix was basically calculated by subtraction of the 2003 mosaic image from the 2015 mosaic image. A 2 × 2 change/no change matrix was used to generate the change detection reports (Table 2).

Matrix elements can be calculated as:

$$X = \begin{pmatrix} A(i = j \cap k = l) & A(i = j \cap k \neq l) \\ A(i \neq j \cap k = l) & A(i \neq j \cap k \neq l) \end{pmatrix} \tag{2}$$

3 Results

Multi-date Landsat images were classified by image segmentation and visual analysis of the segments using high-resolution imagery after co-registration of the satellite

Table 2 Change/no change error matrix [64]

2015 mosaic image	2003 mosaic image		
	No change	Change	Sum
No change	X_{11}	X_{12}	X_{1+}
Change	X_{21}	X_{22}	X_{2+}
Sum	X_{+1}	X_{+2}	1.0

images. Accuracy assessment procedures were applied to measure the quality of the classification processes and an error matrix was produced (Table 3). In total, 144 random points were selected on each of the classified images according to the formula of Fitzpatrick-Lins [65]. The expected accuracy was 90% and allowable error was set to 5%; these conditions required 144 points for reliable results. A stratified random sampling method was used to assign points to all LULC classes on the maps. For equal allocation of samples, the smallest sample size was 5 per class and the largest sample size was 50 per class. An accuracy assessment procedure was applied with the support of field data, aerial photos, prior studies and Google Earth imagery. Overall, the classification accuracy was 93.71% for the 2003 image and 95.04% for the 2015 image.

Producer's accuracy: total number of correct pixels in a category divided by total number of pixels in that category. User's accuracy: division of total number of correct pixels in a category divided by total number of pixels classified in that category. Overall accuracy: total number of correct pixels divided by total number of pixels in the matrix.

3.1 Classified maps

Representative LULC classes for Istanbul Province were defined from Landsat imagery taken in 2003 (Fig. 2) and 2015 (Fig. 3). The USGS land cover class definitions published in 1992, image composites and high-resolution imagery were used to determine LULC classes. Overall, nine classes of USGS 1992 definitions [53] were identified in the study area.

In 2003, areas of vegetation were dispersed in the northern part of Istanbul Province whereas agricultural areas and settlements covered the southern part of the study area. The shorelines of the Marmara Sea and Bosporus were highly populated, as indicated by the densely-packed high intensity residential areas. Another remarkable finding was that the forests and agricultural areas are fragmented by residential areas in both continents of the study area.

Generally, the same LULC patterns observed in 2003 were present in 2015; however, some important differences were detected in the PCC analysis. Increases in settlements and roads, along with decreases in forests, agricultural areas and grasslands were the major differences in the 2015 map; these changes are discussed in detail in the next section of this study.

3.2 LULC change detection

Determination of changes in the thematic land cover maps of the 2003 mosaic and the 2015 mosaic images by a post-classification change detection approach was the final step of this study (Table 4).

Agricultural areas decreased 4.04% from 113,840 ha in 2003 to 109,237 ha in 2015 due to increased settlement activities. Some agricultural areas transitioned to high intensity residential or low intensity residential areas as a result of increased human activity due to the rapid increase in population (Table 5). Forested areas decreased by 3.68%; human activity was the main reason for this ecological destruction, as indicated by conversion of forests to agricultural areas (3.489%), herbaceous plant areas (2.96%) and high intensity residential areas (1.442%).

Another important transition was observed in low intensity residential areas: 28.579% of the low intensity

Table 3 Accuracy assessment matrix for the TM and OLI images

Class name	Landsat TM—2003		Landsat OLI—2015	
	Producers accuracy (%)	Users accuracy (%)	Producers accuracy (%)	Users accuracy (%)
Agriculture	96.15	92.59	92.59	92.59
Bare soil	100.00	75.00	100.00	100.00
Forest	95.24	98.36	98.31	98.31
Herbaceous plants	76.92	76.92	100.00	72.73
High intensity residential	100.00	95.24	96.00	100.00
Low intensity residential	71.43	100.00	66.67	80.00
Roads	100.00	100.00	80.00	100.00
Water	100.00	100.00	100.00	100.00
Wetlands	100.00	50.00	100.00	75.00
Overall class accuracy (%)	93.71		95.04	

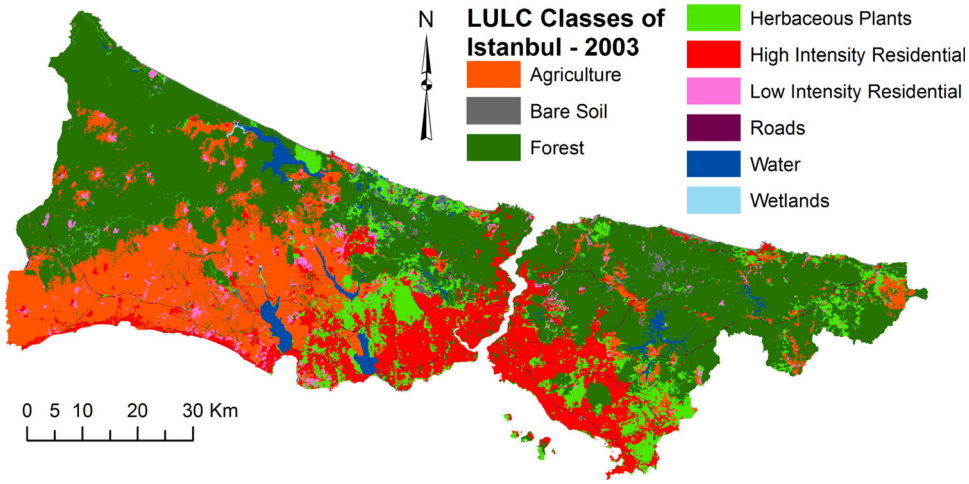

Fig. 2 LULC classes for Istanbul Province in 2003

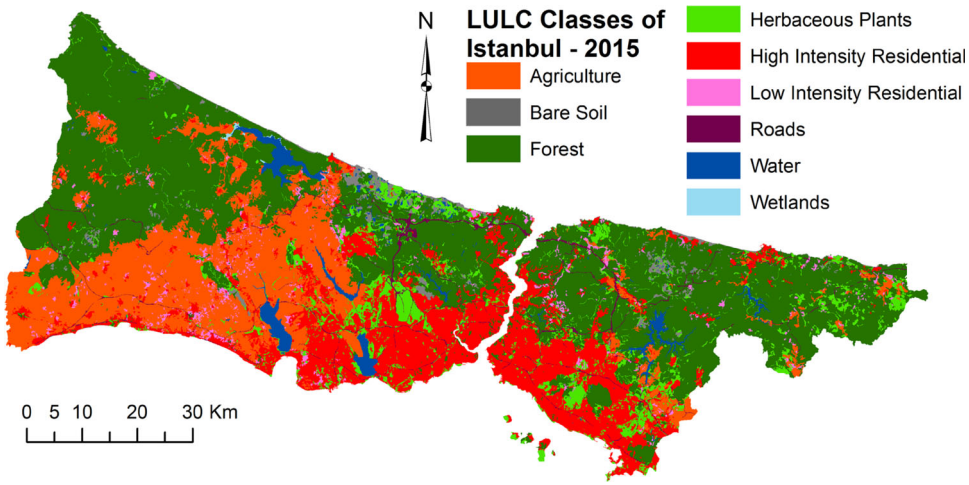

Fig. 3 LULC classes for Istanbul Province in 2015

Table 4 Total LULC changes in Istanbul Province between 2003 and 2015

	2003 (ha)	2015 (ha)	Difference (ha)	Rate (%)
Agriculture	113,840.0	109,237.0	−4603.0	−4.04
Bare soil	6806.5	9663.0	2858.0	41.96
Forest	269,353.0	259,433.0	−9920.0	−3.68
Herbaceous plants	47,538.8	35,082.3	−12,456.5	−26.20
High intensity residential	82,517.9	102,982.0	20,464.1	24.80
Low intensity residential.	11,249.4	11,575,9	3265	2.90
Roads	3098.3	6646.4	3548.1	114.52
Water	12,633.4	12,386.6	−246.8	−2.0
Wetlands	280.3	311.4	31.1	11.1

residential areas converted to high intensity residential areas between 2003 and 2015; these were the places were where most newcomers settled. As previously mentioned, the population of Istanbul increased by about 5 million between 2000 and 2015. Some new residential areas were created for newcomers on previously forested and agricultural areas, but most of the new population settled in existing high intensity residential and low intensity residential areas.

Increased areas of roads was another important change between 2003 and 2015. The area covered by roads by doubled within 15 years: the road density increased in urban areas along with forest destruction in northern parts of the study area for construction of a new highway. In

Table 5 LULC transition matrix for Istanbul between 2003 and 2015 (%)

Final State (2015)	Initial State (2003)								
	Agr	BS	Forest	HP	HIR	LIR	Roads	Water	WL
Agr	80.779	0.758	3.489	9.876	1.740	18.406	6.796	1.398	14.643
BS	0.154	63.834	1.047	3.691	0.157	0.384	0.424	2.963	1.056
Forest	6.547	8.461	89.290	22.751	2.030	11.883	10.711	3.421	4.491
HP	3.715	13.434	2.960	36.465	3.781	6.504	12.960	2.689	1.159
HIR	5.130	6.258	1.442	22.336	90.584	33.645	22.470	0.443	0.000
LIR	3.180	0.596	0.519	2.287	1.030	28.579	1.158	0.046	0.000
Roads	0.385	3.307	1.005	2.090	0.637	0.586	45.449	0.328	0.000
Water	0.077	3.267	0.200	0.481	0.026	0.014	0.031	88.410	41.280
WL	0.033	0.000	0.047	0.012	0.000	0.000	0.000	0.301	37.370
CT	100.000	100.000	100.000	100.000	100.000	100.000	100.000	100.000	100.000
CC	19.221	36.166	10.710	63.535	9.416	71.421	54.551	11.590	62.630

Agr agriculture, *BS* bare soil, *HP* herbaceous plants, *HIR* high intensity residential, *LIR* low intensity residential, *WL* wetlands, *CT* class total, *CC* class changes

total, 2529.89 ha of forested area was destroyed for construction of the new highway; this area represents 0.46% of the total area of Istanbul Province. Additionally, bare soil areas increased markedly, especially due to mining activities in forested areas of northern Istanbul; these activities contributed to a decrease in the green cover area of the study area.

A LULC difference map (Fig. 4) was created by subtraction of LULC classes in the 2003 mosaic image from the 2015 mosaic image. The subtraction was applied to every corresponding pixel in the images; and differences of more than 20% were classified as "change places". Red and blue areas indicate positive and negative changes while light grey areas underwent no change. Difference maps are usually generated by subtraction of unclassified satellite imagery and increase and decrease areas show amount of changes in pixel values satellite images. Pixel values of satellite imagery are usually high in urbanized areas and bare soils and positive changes can be understood as vegetation loss and deforestation. The difference map shown below was prepared by subtraction of classified imagery. That means order of LULC classes on classified maps affected type of change in unmeaningful way. Therefore areas of changes should be considered more than type of change as negative of positive. As shown in the map, changes in LULC classes were observed thorough the entirety of Istanbul Province; these changes were more obvious in the centre of the European part that was mostly covered by agricultural areas in 2003. Both agricultural areas and forest areas became fragmented by different LULC classes, as indicated by the small, thin areas of change. The new highway appears very distinctively as the thick red line throughout the centre of Istanbul and represents the strongest proof of deforestation due to human activities.

4 Discussion

LULC change analysis in Istanbul Province was achieved by: (1) classification of Landsat imagery using USGS 1992 land cover class definitions, (2) comparison of classified Landsat data in images captured in 2003 and 2015, and (3) quantification of LULC classes in the before and after images (using the method of Yuan et al. [66]). In the context of determining LULC change detection over time, this study demonstrates the potential of these techniques for producing accurate land cover maps from Landsat imagery compared to the lower accuracy of pixel based methods [16]. Moreover, a number of significant LULC changes were detected in the study area between 2003 and 2105 that merit further discussion.

Using pixel-based classification techniques, it is almost impossible to separate urban areas from bare soils, mines, beaches or fallow fields if the data is generated from a 30 m resolution satellite image such as Landsat TM images. After supervised or unsupervised classification, masking of incorrectly classified areas and secondary classification is advised to overcome this issue. However, even after applying all of the recommended techniques, it is not possible to acquire a map with 95% accuracy using Landsat imagery which is accomplished in this study by visual analysis and editing of vector segments.

The improved classification accuracy of the image segmentation approach over pixel-based classification is an important finding of this study. Image segmentation has the

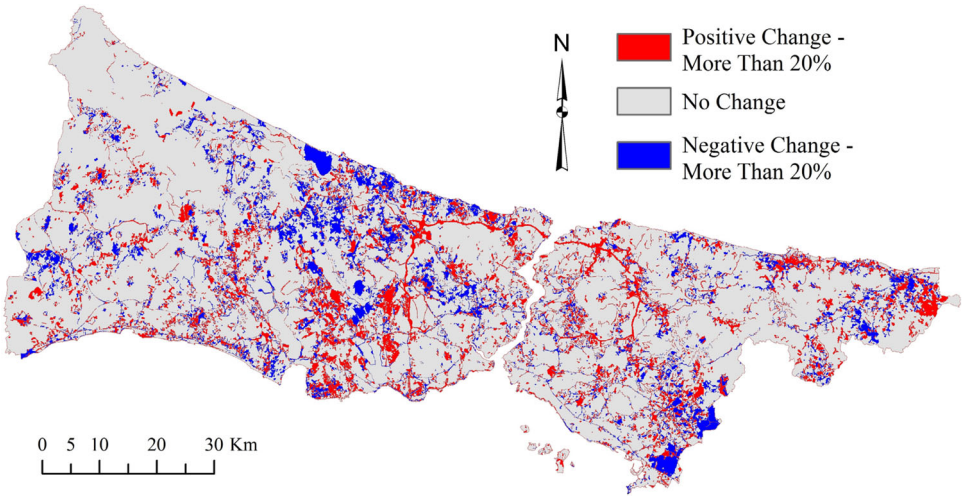

Fig. 4 Map of LULC changes in Istanbul between 2003 and 2015. *Red* and *blue* areas indicate positive and negative changes; *light grey* areas underwent no change. (Color figure online)

advantage of considering the spatial characteristics of objects along with their spectral features. A multi-resolution segmentation approach was initially applied in this study. A secondary segmentation such as spectral difference segmentation could have been applied to decrease the number of existing segments, but resulted in similar issues as pixel-based classification. Large segments produced by spectral difference segmentation covered both bare soils and urban areas. Therefore, the segments generated by multi-resolution segmentation were classified by visual analysis and the secondary segmentation was ignored. More than 20,000 segments were classified with the help of high-resolution satellite imagery, Google Earth and analogue maps. The results acquired using this hybrid GIS–RS method are very promising: normally it is very difficult to obtain maps that are more than 90% accurate using mid-resolution (30 m) resolution Landsat images. However, manual classification of the segments by visual analysis achieved remarkable accuracy for both the 2003 and 2015 images (93.71 and 95.04%, respectively).

The object-based approach also provides an advantage with respect to atmospheric corrections. Satellite imagery frequently have dark individual pixels distributed throughout the entire image. This type of unwanted atmospheric effect can be eliminated by a number of filtering techniques, but filtering can affect the entire image and change the original digital data. However, these pixels could be detected individually and corrected manually using the segmentation approach.

We suggest that image segmentation should not be applied to images with a higher than 8-bit radiometric resolution if another segmentation method will not be applied to decrease the number of segments and visual analysis will be selected as the classification method. Otherwise, millions of segments would be produced by the software; such a high number of segments would be completely useless for classification by visual analysis. As a result, object-based classification can be considered as a time-consuming but very accurate approach for satellite image classification.

5 Conclusions

Population growth due to migration has led to important changes in Istanbul Province between 2003 and 2015. The post-classification comparison revealed a dramatic increase in high intensity residential areas. Agricultural areas, water, roads and forested lands changed less significantly, though 6195 ha of forested lands and 3802 ha agricultural areas were lost over the 12-year period, and these areas are very important for the ecological biodiversity of Istanbul Province. Moreover, while road network expansion is generally a good thing for a city, the road network expansion in Istanbul Province during last the 12 years came at the cost of forestland destruction.

Overall, this study demonstrates that the vegetation cover and biodiversity of Istanbul have decreased in the last 12 years due to human activities that could have been avoided or mitigated. At a minimum, the new road construction could have been achieved with minimal damage to forest areas (or even without their destruction) by applying modern technological developments. Furthermore, as Istanbul Province already has more than 15 million inhabitants, local and central government representatives should take note of these findings and develop political strategies that discourage migration to the city and preserve its natural habits and ecological biodiversity.

References

1. Monela, G., & Solberg, B. (1998). Deforestation rate and land use/land cover changes in rainforest of the Nguru mountains,

Tanzania. *Faculty of Forest Record, 68,* 14. **(Sokoine University of Agriculture, Morogoro, Tanzania)**.
2. Estoque, R. C., & Murayama, Y. (2011). Spatio-temporal urban land use/cover change analysis in a hill station: The case of Baguio City, Philippines. *Procedia Social and Behavioral Sciences, 21,* 326–335.
3. Braimoh, K. A., & Onishi, T. (2007). Spatial determinants of urban land use change in Lagos, Nigeria. *Land Use Policy, 24,* 502–515.
4. Foody, G. M. (2001). Monitoring the magnitude of land-cover change around the southern limits of Sahara. *Photogrammetric Engineering and Remote Sensing, 56*(11), 1515–1522.
5. Lambin, E. F., Rounsevell, M. D. A., Geist, H. J., et al. (2000). Are agricultural land-use modelsable to predict changes in land-use intensity? *Agriculture, Ecosystems and Environment, 82,* 321–331.
6. Cihlar, J., & Jansen, L. J. M. (2001). From land cover to land-use: A methodology for efficient land-use mapping over large areas. *The Professional Geographer, 53*(2), 275–289.
7. Slayback, D. (2003). Landcover change in the Takamanda forest reserve, Cameroon: 1986–2000. In J. A. Chomiskey & T. C. H. Sunderland's (Eds.), *Takamanda: The biodiversity of an African rainforest*. Washington, DC: Smithsonian Institution. **(SI/MAB Series #8)**.
8. Turner, M. D. (2003). Environmental science and social causation in the analysis of Sahelian pastoralism. In K. S. Zimmerer & T. J. Basset's (Eds.), *Political ecology: An integrative approach to geography and environment-development studies*. New York: Guilford Press.
9. DeVries, B., Decuyper, M., Verbesselt, J., Zeileis, A., Herold, M., Joseph, S., et al. (2015). Tracking disturbance-regrowth dynamics in tropical forests using structural change detection and Landsat time series. *Remote Sensing of Environment, 169,* 320–334.
10. Kabba, V. T. S., & Li, J. (2011). Analysis of land use and land cover changes and their ecological implications in Wuhan, China. *Journal of Geography and Geology, 3,* 1.
11. Kashaigili, J. J., & Majaliwa, A. M. (2010). Integrated assessment of land use and cover changes in the Malagarasi river catchment in Tanzania. *Physics and Chemistry of the Earth, 35*(730), 741.
12. Hermosilla, T., Wulder, M. A., White, J. C., Coops, N. C., Hobart, G. W., et al. (2015). Regional detection, characterization, and attribution of annual forest change from 1984 to 2012 using Landsat-derived time-series metrics. *Remote Sensing of Environment, 170,* 121–132.
13. Rokni, K., Ahmad, A., Solaimani, K., Hazini, S., et al. (2015). A new approach for surface water change detection: Integration of pixel level image fusion and image classification techniques. *International Journal of Applied Earth Observation and Geoinformation, 34,* 226–234.
14. De Beurs, K. M., Henebry, G. M., Owsley, B. C., Sokolik, I., et al. (2015). Using multiple remote sensing perspectives to identify and attribute land surface dynamics in Central Asia 2001–2013. *Remote Sensing of Environment, 170,* 48–61.
15. Bouchaffra, D., Cheriet, M., Jodoin, P. M., Beck, D., et al. (2015). Machine learning and pattern recognition models in change detection. *Pattern Recognition, 48,* 613–615.
16. Dewan, M. A., & Yamaguchi, Y. (2009). Using remote sensing and GIS to detect and monitor land use and land cover change in Dhaka Metropolitan on Bangladesh during 1960–2005. *Environmental Monitoring and Assessment, 150,* 237–249.
17. Wan, L., Zhang, Y., Qi, S., Na, X., et al. (2015). Comparison of land use/land cover change and landscape patterns in Honghe National Nature Reserve and the surrounding Jiansanjiang Region, China. *Ecological Indicators, 51,* 205–214.
18. Van de Voorde, T., van der Kwast, J., Poelmans, L., Canters, F., Binard, M., Cornet, Y., et al. (2016). Projecting alternative urban growth patterns: The development and application of a remote sensing assisted calibration framework for the Greater Dublin Area. *Ecological Indicators, 60,* 1056–1069.
19. Elbeih, S. F., & Soliman, N. M. A. (2015). An approach to locate and map swelling soils around Sohag—Safaga road, Eastern Desert, Egypt using remote sensing techniques for urban development. *The Egyptian Journal of Remote Sensing and Space Science, 18*(1), 31–41. **(supplement 1)**.
20. Willis, K. S. (2015). Remote sensing change detection for ecological monitoring in United States protected areas. *Biological Conservation, 182,* 233–242.
21. Gandhi, G. M., Parthiban, S., Thummalu, N., Christy, A., et al. (2015). NDVI: Vegetation change detection using remote sensing and GIS—a case study of Vellore District. *Procedia Computer Science, 57,* 1199–1210.
22. Motohka, T., Shimada, M., Uryu, Y., Setiabudi, B., et al. (2014). Using time series PALSAR gamma nought mosaics for automatic detection of tropical deforestation: A test study in Riau, Indonesia. *Remote Sensing of Environment, 155,* 79–88.
23. Reiche, J., Verbesselt, J., Hoekman, D., Herold, M., et al. (2015). Fusing Landsat and SAR time series to detect deforestation in the tropics. *Remote Sensing of Environment, 156,* 276–293.
24. Sun, D. (2015). Detection of dryland degradation using Landsat spectral unmixing remote sensing with syndrome concept in Minqin County, China. *International Journal of Applied Earth Observation and Geoinformation, 41,* 34–45.
25. Soto, I. M., Cannizzaro, J., Muller-Karger, F. E., Hu, C., Wolny, J., Goldgof, D., et al. (2015). Evaluation and optimization of remote sensing techniques for detection of Karenia brevis blooms on the West Florida Shelf. *Remote Sensing of Environment, 170,* 239–254.
26. Jensen, J. R. (1996). *Introductory digital image processing: A remote sensing perspective* (2nd ed., p. 316). New York: Prentice Hall.
27. Volpi, M., Tuia, D., Bovolo, F., Kanevski, M., Bruzzone, L., et al. (2013). Supervised change detection in VHR images using contextual information and support vector machines. *International Journal of Applied Earth Observation and Geoinformation, 20,* 77–85.
28. Hussain, M., Chen, D., Cheng, D., Wei, H., Stanley, D., et al. (2013). Change detection from remotely sensed images: From pixel-based to object-based approaches. *ISPRS Journal of Photogrammetry and Remote Sensing, 80,* 91–106.
29. Fan, J., Zhang, J., Mei, K., Peng, J., Gao, L., et al. (2015). Cost-sensitive learning of hierarchical tree classifiers for large-scale image classification and novel category detection. *Pattern Recognition, 48,* 1673–1687.
30. Xiaolu, S., & Bo, C. (2011). Change detection using change vector analysis from Landsat TM images in Wuhan. *Procedia Environmental Sciences, 11,* 238–244.
31. Pekel, J. F., Vancutsem, C., Bastin, L., Clerici, M., Vanbogaert, E., Bartholomé, E., et al. (2014). A near real-time water surface detection method based on HSV transformation of MODIS multi-spectral time series data. *Remote Sensing of Environment, 140,* 704–716.
32. Zhang, Z., Chen, H., Xu, Y., Zhong, J., Lv, N., Chen, S., et al. (2015). Multisensor-based real-time quality monitoring by means of feature extraction, selection and modeling for Al alloy in arc welding. *Mechanical Systems and Signal Processing, 60–61,* 151–165.
33. Yang, X. T., Liu, H., Gao, X., et al. (2015). Land cover changed object detection in remote sensing data with medium spatial resolution. *International Journal of Applied Earth Observation and Geoinformation, 38,* 129–137.
34. Gärtner, P., Förster, M., Kurban, A., Kleinschmit, B., et al. (2014). Object based change detection of Central Asian Tugai

vegetation with very high spatial resolution satellite imagery. *International Journal of Applied Earth Observation and Geoinformation, 31,* 110–121.
35. Taha, L. G. E. (2014). Assessment of urbanization encroachment over Al-Monib island using fuzzy post classification comparison and urbanization metrics. *The Egyptian Journal of Remote Sensing and Space Science, 17,* 135–147.
36. Colditz, R. R., Acosta-Velázquez, J., Díaz Gallegos, J. R., Vázquez Lule, A. D., Rodríguez-Zúñiga, M. T., Maeda, P., et al. (2012). Potential effects in multi-resolution post-classification change detection. *International Journal of Remote Sensing, 33,* 6426–6445.
37. Teng, S. P., Chen, Y. K., Cheng, K. S., Lo, H. C., et al. (2008). Hypothesis-test-based landcover change detection using multitemporal satellite images—a comparative study. *Advances in Space Research, 41,* 1744–1754.
38. Turkish Statistical Institute (TUIK), 2016. Address based population registration system results. Accessed February 25, 2015, http://tuikapp.tuik.gov.tr/adnksdagitapp/adnks.zul?dil=2.
39. Istanbul Metropolitan Municipality (IMM), 2015. Geographical and strategic position of Istanbul. Accessed September 11, 2015, http://www.ibb.gov.tr/sites/ks/en-US/0-Exploring-The-City/Location/Pages/GeographicalandStrategicPosition.aspx.
40. Turkish State Meteorological Service (TSMS), 2015. Annual total precipitation data of Istanbul. Accessed September 11, 2015, http://www.mgm.gov.tr/veridegerlendirme/yillik-toplam-yagis-verileri.aspx?m=istanbul#sfB.
41. Mas, J. F. (1999). Monitoring land-cover changes: A comparison of change detection techniques. *International Journal of Remote Sensing, 20*(1), 139–152.
42. Hexagon Geospatial, (2016). Radiometric enhancement, histogram matching. Accessed February 24, 2016, https://wiki.hexagongeospatial.com//index.php?title=Radiometric_Enhancement.
43. USGS (United States Geological Survey), 2015a. Band designations for the Landsat satellites. Accessed August 15, 2015, http://landsat.usgs.gov/band_designations_landsat_satellites.php.
44. Song, C., Woodcock, C. E., Seto, K. C., Lenney, M. P., Macomber, S. A., et al. (2001). Classification and change detection using Landsat TM data: When and how to correct atmospheric effects? *Remote Sensing of Environment, 75,* 230–244.
45. Jensen, J. R. (1983). Urban/suburban land use analysis. *Manual Remote Sensing, 2,* 1571–1666.
46. Makkaesorn, A., Chang, N.-B., Li, J., et al. (2009). Seasonal change detection of riparian zones with remote sensing images and genetic programming in a semi-arid watershed. *Journal of Environmental Management, 90,* 1069–1080.
47. Mei, A., Manzo, C., Fontinovo, G., Bassani, C., Allegrini, A., Petracchini, F., et al. (2015). Assessment of land cover changes in Lampedusa Island (Italy) using Landsat TM and OLI data. *Journal of African Earth Sciences, 122,* 15–24.
48. El-Asmar, H. M., Hereher, M. E., El Kafrawy, S. B., et al. (2013). Surface area change detection of the Burullus Lagoon, North of the Nile Delta, Egypt, using water indices: A remote sensing approach. *The Egyptian Journal of Remote Sensing and Space Science, 16,* 119–123.
49. Lillesand, T., Kiefer, R., Chipman, J., et al. (2004). *Remote sensing and image interpretation* (5th ed.). New York: Wiley.
50. Baatz, M., & Schaepe, A. (2000). Multi resolution segmentation: An optimization approach for high quality multi-scale image segmentation. In J. Strobl & T. Blaschke (Eds.), *Angewandte geographische informations verarbeitung* (Vol. XII, pp. 12–23). Heidelberg: Wichmann.
51. Definiens (2003). Definiens imaging, eCognition. Resource document. Harris Geospatial. Accessed September 12 , 2015, http://www.definiens-imaging.com.
52. Forghani, A., Cechet, B., Nadimpalli, K., et al. (2007). Object-based classification of multi-sensor optical imagery to generate terrain surface roughness information for input to wind risk simulation. In *IEEE international geoscience and remote sensing symposium, IGARSS 2007*, Barcelona.
53. USGS (United States Geological Survey), 2015b. NLCD 92 land cover class definitions. Accessed September 12, 2015, http://landcover.usgs.gov/classes.php.
54. Jensen, J. R. (2005). *Introductory digital image processing: A remote sensing perspective* (3rd ed.). New Jersey: Pearson Education Inc.
55. Zhan, X., Sohlber, R. A., Townshend, J. R. G., DiMiceli, C., Carroll, M. L., Eastman, J. C., et al. (2002). Detection of land cover changes using MODIS 250 m data. *Remote Sensing of Environment, 83,* 336–350.
56. Grinblat, G. L., Uzal, L. C., Granitto, P. M., et al. (2013). Abrupt change detection with one-class time-adaptive support vector machines. *Expert Systems with Applications, 40,* 7242–7249.
57. Ngo, L. T., Mai, D. S., Pedrycz, W., et al. (2015). Semi-supervising interval Type-2 Fuzzy C-Means clustering with spatial information for multi-spectral satellite image classification and change detection. *Computers and Geosciences, 83,* 1–16.
58. Afify, H. A. (2011). Evaluation of change detection techniques for monitoring land-cover changes: A case study in new Burg El-Arab area. *Alexandria Engineering Journal, 50,* 187–195.
59. Kleynhans, W., Salmon, B. P., Olivier, J. C., et al. (2015). Detecting settlement expansion in South Africa using a hyper-temporal SAR change detection approach. *International Journal of Applied Earth Observation and Geoinformation, 42,* 142–149.
60. Singh, A. (1989). Review article digital change detection techniques using remotely sensed data. *International Journal of Remote Sensing, 10*(6), 989–1003.
61. Lê, T. T., Atto, A. M., Trouvé, E., Solikhin, A., Pinel, V., et al. (2015). Change detection matrix for multitemporal filtering and change analysis of SAR and PolSAR image time series. *ISPRS Journal of Photogrammetry and Remote Sensing, 107,* 64–76.
62. Qi, Z., Yeh, A. G.-O., Li, X., Zhang, X., et al. (2015). A three-component method for timely detection of land cover changes using polarimetric SAR images. *ISPRS Journal of Photogrammetry and Remote Sensing, 107,* 3–21.
63. Biging, G. S., Colby, D. R., & Congalton, R. G. (1998). Sampling systems for change detection accuracy assessment. In R. S. Lunetta & C. D. Elvidge (Eds.), *Remote sensing change detection: Environmental monitoring methods and applications* (pp. 281–308). Chelsea, Michigan: Sleeping Bear Press.
64. Van Oort, P. A. J. (2007). Interpreting change detection error matrix. *Remote Sensing of Environment, 108,* 1–8.
65. Fitzpatrick-Lins, K. (1981). Comparison of sampling procedures and data analysis for a land-use and lond-cover map. *Photogrammetric Engineering and Remote Sensing, 47*(3), 343–351.
66. Yuan, F., Sawaya, K. E., Loeffelholz, B. C., & Bauer, M. E. (2015). Land cover classification and change analysis of the Twin Cities (Minnesota) metropolitan area by multitemporal Landsat remote sensing. *Remote Sensing of Environment, 98,* 317–328.